ACS OMEGA

http://pubs.acs.org/journal/acsodf

Article

Maltotriose–Chlorin e6 Conjugate Linked *via* Tetraethyleneglycol as an Advanced Photosensitizer for Photodynamic Therapy. Synthesis and Antitumor Activities against Canine and Mouse Mammary Carcinoma Cells

Atsushi Narumi,* Rioko Rachi, Hiromi Yamazaki, Seigou Kawaguchi, Moriya Kikuchi, Hiroyuki Konno, Tomohiro Osaki,* Yoshiharu Okamoto, Xiande Shen, Toyoji Kakuchi, Hiromi Kataoka, Akihiro Nomoto, Tomokazu Yoshimura, and Shigenobu Yano

Cite This: *ACS Omega* 2021, 6, 7023–7033

Read Online

ACCESS | Metrics & More | Article Recommendations | Supporting Information

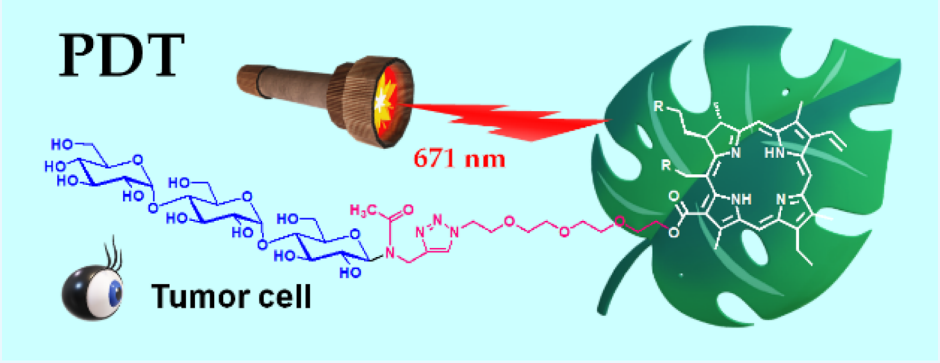

ABSTRACT: Glycoconjugated chlorins represent a promising class of compounds that meet the requirements for the third-generation photosensitizer (PS) for photodynamic therapy (PDT). We have focused on the use of glucose (Glc) to improve the performance of the PS based on the Warburg effect—a phenomenon where tumors consume higher Glc levels than normal cells. However, as a matter of fact, Glc-conjugation has a poor efficacy in hydrophilic modification; thus, the resultant PS is not suitable for intravenous injection. In this study, a Glc-based oligosaccharide, such as maltotriose (Mal_3), is conjugated to chlorin e6 (Ce6). The conjugation is assisted by two additional molecular tools, such as propargyl amine and a tetraethylene glycol (TEG) derivative. This route produced the target Mal_3–Ce6 conjugate linked *via* the TEG spacer (Mal_3–TEG–Ce6), which shows the required photoabsorption properties in the physiological media. The PDT test using canine mammary carcinoma (SNP) cells suggested that the antitumor activity of Mal_3–TEG–Ce6 is extremely high. Furthermore, *in vitro* tests against mouse mammary carcinoma (EMT6) cells have been demonstrated, providing insights into the photocytotoxicity, subcellular localization, and analysis of cell death and reactive oxygen species (ROS) generation for the PDT system with Mal_3–TEG–Ce6. Both apoptosis and necrosis of the EMT6 cells occur by ROS that is generated *via* the photochemical reaction between Mal_3–TEG–Ce6 and molecular oxygen. Consequently, Mal_3–TEG–Ce6 is shown to be a PS showing the currently desired properties.

INTRODUCTION

Photodynamic therapy (PDT) has increasingly attracted much attention as a minimally invasive cancer therapy.[1−4] A brief overview of the therapy is that a photosensitizer (PS) is administered to the body by an intravenous injection and the cancer tissues are irradiated by visible red light. The photochemical reaction between PS and tissue oxygen (O_2) occurs according to the mechanism described by the Jablonski diagram, eventually generating reactive oxygen species (ROS) that kill the target cell. Thus, the molecular properties of PS determine the performance of PDT, which require (a) strong photoabsorption of visible light in the longer wavelength region that is likely to penetrate deeper into tissues, (b) high ROS generation ability, (c) selective accumulation ability to the inside of the target tumor cells, (d) no toxicity in the dark, and (e) rapid clearance out of the body after the treatment. In clinical use, (f) compatibility with the physiological media

Received: December 29, 2020
Accepted: February 24, 2021
Published: March 8, 2021

https://dx.doi.org/10.1021/acsomega.0c06316
ACS Omega 2021, 6, 7023–7033

Chart 1. Synthetic Conception in Which Maltotriose (Mal_3) Is Covalently Bonded with Chlorin e6 Dimethyl Ester (Ce6−DME) Assisted by Using Two Molecular Tools, Such as PA and the TEG Derivative, to Produce the Mal_3−Ce6 Conjugate Linked with the TEG-Spacer (Mal_3−TEG−Ce6).

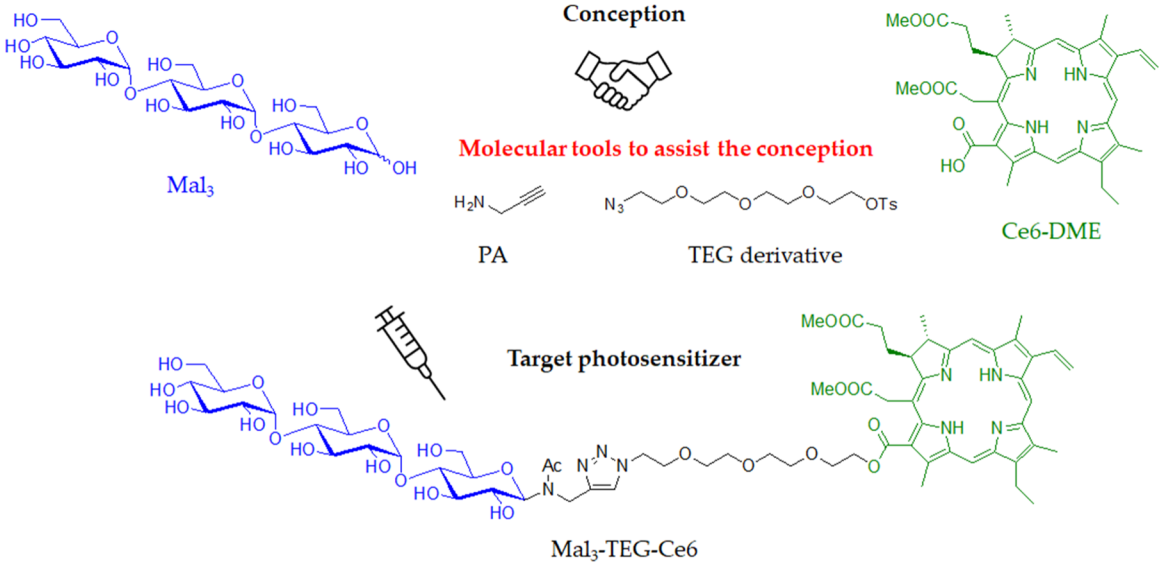

(water-solubility) is added as a crucial property, which allows the administration of PS by intravenous injection without any toxic organic solvents and solubilizing agents that cause side effects.

Dehydroporphyrins, called chlorins, are a class of molecules satisfying the properties of the (a) strong photoabsorption and (b) high ROS generation ability. Representatively, 5,10,15,20-tetrakis(3-hydroxyphenyl)chlorin (Temoporfin, Foscan) is categorized as a chlorin-type PS, which is artificially synthesized from commercially available chemicals.[5] Alternatively, mono-l-aspartyl chlorin e6 (NPe6, Talaporfin, Laserphyrin)[6] is a PS derived from naturally occurring chlorophylls *a*. Pyropheophorbide-*a* analogues[7] are also categorized as a PS that originate from natural dyes. A prime trend for the PS development is currently directed to utilize the ability of some other biologically active molecules to improve the requirement (c) selective accumulation ability to the inside of the target tumor cells. The light-sensitive drug in which the accumulation ability is intentionally enhanced by the incorporation of bioactive molecules is distinguished as "the third-generation PS". A highlighted approach includes glycoconjugation.[1,3] Saccharides are covalently bonded to the photoactive molecules derived from artificial chlorin dyes.[8−22] As an example, a chlorin derivative possessing four perfluorinated aromatic rings encircled with four glucose (Glc) molecules has been synthesized. The product, called G−chlorin, shows a high photocytotoxicity with a half-maximal (50%) inhibitory concentration (IC_{50}) value of less than 0.5 μM.[14] The anticancer effects of G−chlorin for gastric and colon cancer have been reported to be high.[16] These results strongly suggest that the Warburg effect[23]—a phenomenon where tumors consume higher Glc levels than normal cells—can be utilized in the conception to develop the third-generation PS. Naturally occurring chlorin derivatives are also targeted for glycoconjugation.[24−30] Recently, chlorin e6 (Ce6) has been decorated with Glc to develop a new family of PS (Glc−Ce6), which shows an extremely high photocytotoxicity.[27,28] Ce6 is a molecule that is derived from naturally occurring chlorophyll *a*; therefore, G−Ce6 is expected to show an improved biocompatibility and body clearance, meeting the requirements of both (d) no toxicity in the dark and (e) rapid clearance out of the body after the treatment. However, as a matter of fact, G−Ce6 is insoluble in water due to the strong hydrophobic property of the Ce6 unit. This result suggested that the strong hydrophobic property of the Ce6 unit dominates the solubility of G−Ce6. Another plausible reason is that the molecular size of Glc is small compared to that of Ce6 composed of the tetrapyrrole ring. Eventually, the Ce6 moiety is not sufficiently covered by hydrophilic moieties in the aqueous media, resulting in G−Ce6 forming precipitates. Thus, satisfying the requirement (f) compatibility with the physiological media (water-solubility) is the next challenge for the PDT with the glycoconjugated Ce6.

In this study, maltotriose (Mal_3), a Glc-based trisaccharide, is conjugated to Ce6 to develop an advanced PS, showing both high performance and water solubility. Malto-oligosaccharide (Mal_n) is a general term for the oligosaccharides consisting of Glc as the repeating units, which are known to be found in a syrup as the main components. Mal_n exhibits not only the Warburg effect derived from the Glc unit but also the stronger and well-defined hydrophilic property due to possessing multiple and definite numbers of hydroxyl groups; thus, they are special molecules in bioconjugated chemistry and pharmacology. Indeed, we have previously reported that the Mal_3-conjugation provides a very positive result for the preparation of the water-soluble PS.[20,21] Chart 1 depicts a synthetic conception in this study in which Mal_3 is covalently linked to the Ce6 dimethyl ester (Ce6−DME) in which the connection is assisted by two other molecular tools such as propargyl amine (PA) and the tetraethylene glycol (TEG) derivative. The synthesis is achieved by three reaction steps staring from Mal_3 without tedious protection/deprotection processes, which consist of (i) the direct *N*-glycosylation reaction, (ii) the copper-catalyzed azide/alkyne "click" (CuAAC) reaction, and (iii) the S_N2 esterification reaction. The structure of the final product is assignable to the Mal_3−Ce6 conjugate linked *via* the TEG spacer (Mal_3−TEG−Ce6), which shows water solubility and characteristic photo-

https://dx.doi.org/10.1021/acsomega.0c06316
ACS Omega 2021, 6, 7023−7033

Scheme 1. Synthesis of the Mal_3−Ce6 Conjugate Linked *via* the TEG Spacer (Mal_3−TEG−Ce6)

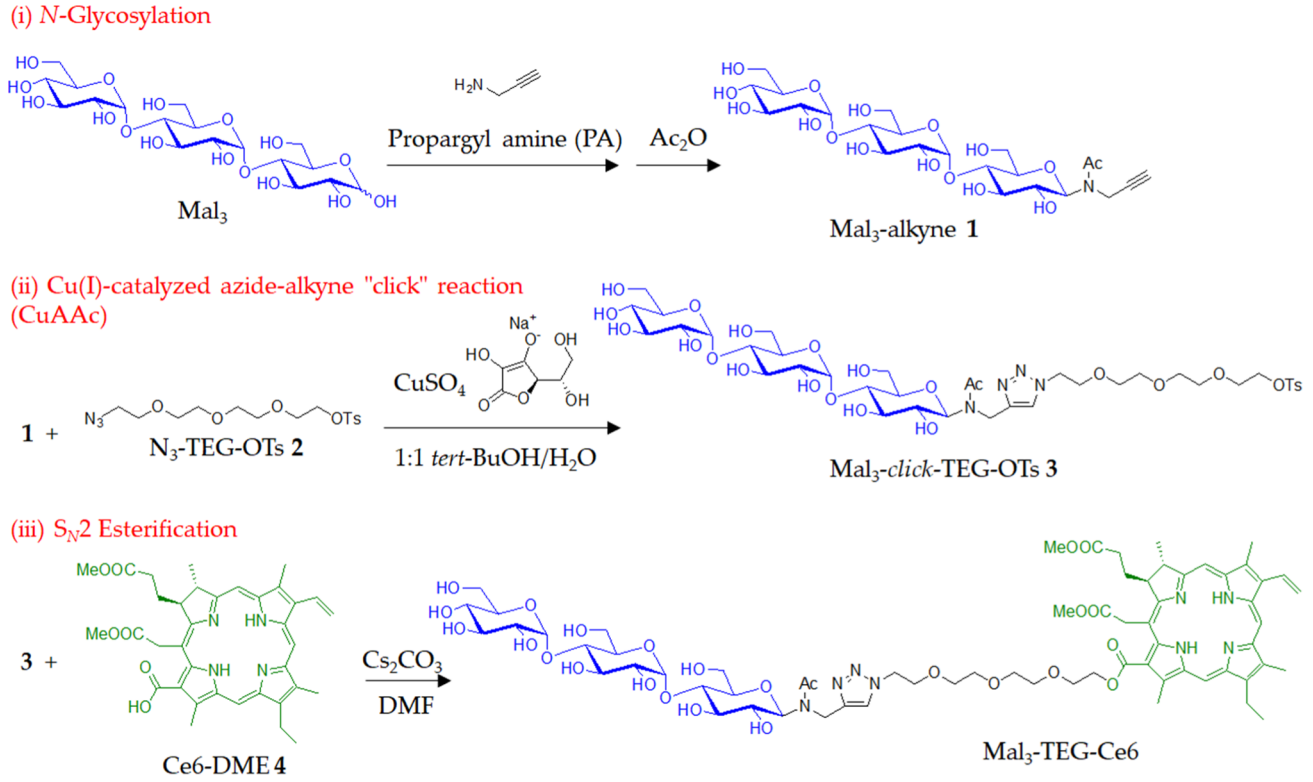

absorption properties at the longer wavelength in the visible-light area in aqueous physiological media. The performance of Mal_3−TEG−Ce6 is clarified by the antitumor test against canine mammary carcinoma (SNP) cells, whose performance is compared to that of the previously reported glucose−Ce6 conjugate (G−Ce6). We also report the photocytotoxicity, subcellular localization, analysis of cell death, and ROS generation for the Mal_3−TEG−Ce6 PDT system using mouse mammary carcinoma (EMT6) cells.

RESULTS AND DISCUSSION

Synthesis of the Maltotriose−Chlorin e6 Conjugate (Mal_3−TEG−Ce6). A synthetic protocol for the target PS is shown in Scheme 1. We performed the *N*-glycosylation reaction of PA to maltotriose (Mal_3) according to a similar method described in the literature.[31] The reaction produced Mal_3 with an ethynyl group (Mal_3−alkyne **1**), which was then reacted with TEG with azido and tosylate groups[32] (N_3−TEG−OTs **2**) using $CuSO_4$ and sodium L-ascorbate to produce a product **3**. It should be noted that this CuAAC reaction had to be performed before the conjugation with the chlorin derivative in order to avoid the contamination of the metal species for the final PS. Figure 1a shows the ^{1}H NMR spectrum of **3** in D_2O, exhibiting the signals due to the protons of the triazole ring (8.00 and 7.77 ppm), the aromatic ring (7.67 and 7.32 ppm), the Mal_3 and TEG units (5.45−3.24 ppm), the methyl group (2.28 ppm), and the *N*-acetyl group (2.08 and 1.95 ppm). The sharp peak due to the azido group (2262 cm^{-1}) is observed in the IR spectrum of **2** (Figure S1), while completely absent in that of **3** (Figure S2). Alternatively, the large peaks due to hydroxyl groups (3700−3000 cm^{-1}) and acetyl group (1732 cm^{-1}) are present in the IR spectrum of **3** (Figure S2). The signals observed for the ^{13}C NMR spectrum were fully assigned (Figure S4). These results support that **3** is assignable to the target Mal_3−TEG−OTs.

We finally performed the S_N2 esterification reaction between **3** and the chlorin e6 dimethyl ester derivative (Ce6−DME **4**) using Cs_2CO_3 in dry *N*,*N*-dimethylformamide at room temperature. The residue from the reaction mixture was purified by column chromatography to isolate the product. Figure 1b shows the ^{1}H NMR spectrum of the product in DMSO-d_6, displaying signals due to the protons derived from the **3** unit, such as the triazole ring (8.01 and 7.85 ppm), the Mal_3−TEG unit (5.46−3.06 ppm), and the *N*-acetyl group (2.07 and 1.93 ppm). Additionally, the characteristic resonances due to the protons in the Ce6 unit (H_{chl}s) distinctly appear, which include H_{chl}-10, H_{chl}-5, H_{chl}-20, H_{chl}-3^1, H_{chl}-3^2, H_{chl}-15^1, H_{chl}-18, H_{chl}-17, H_{chl}-8^1, H_{chl}-17^2, H_{chl}-17^1, H_{chl}-8^2, H_{chl}-18^1, H_{chl}-21, and H_{chl}-23. The area integration values for the respective signals are in good agreement with the target structures. The signals observed for the ^{13}C NMR spectrum have been fully assigned (Figure S5). HR-ESI-MS exhibited the main peak at *m*/*z* 1431.60547, which agreed with the calculated $[M + Na]^+$ ion peak value for the target compound of 1431.60713. These results indicated that the S_N2 esterification reaction between the OT group of **3** and the COOH group of **4** proceeded to produce the target PS such as the Mal_3−Ce6 conjugate linked *via* the TEG spacer (Mal_3−TEG−Ce6).

Water Solubility. The desired result obtained was that Mal_3−TEG−Ce6 readily dissolved in water, producing a green aqueous solution. The water solubility was determined to be >11.6 mg mL^{-1}. We determined the partition coefficient (log *P*) to quantify the introduced hydrophilicity that is defined by eq 1

$$\log P = \log([C_{octanol}]/[C_{PBS}]) \quad (1)$$

https://dx.doi.org/10.1021/acsomega.0c06316
ACS Omega 2021, 6, 7023−7033

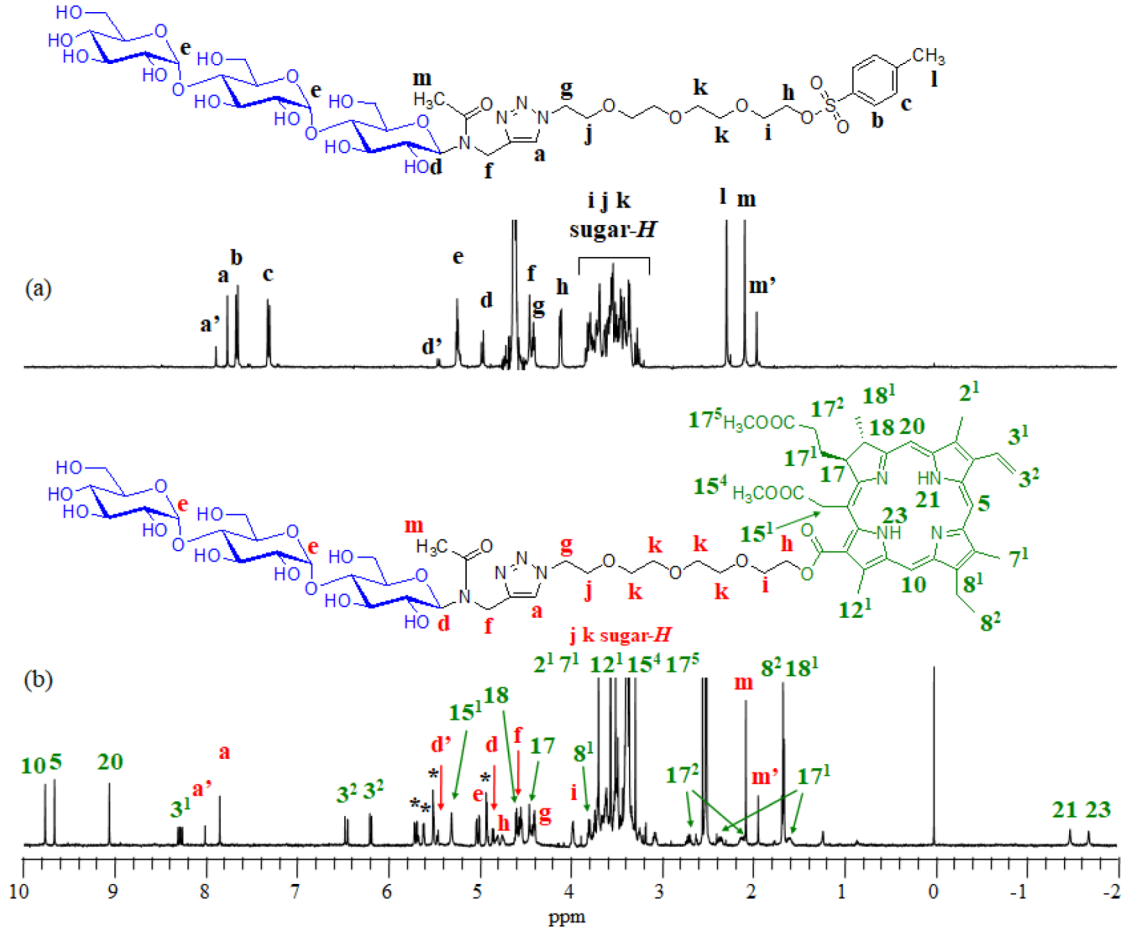

Figure 1. ^{1}H NMR spectra of (a) **3** in D_2O and (b) Mal_3−TEG−Ce6 in DMSO-d_6 (the symbol * in the spectra corresponds to the protons due to the hydroxyl groups).

Table 1. Summary for Photoabsorption Properties of 4 in DMSO (Control) and Mal_3−TEG−Ce6 in DMSO and PBS

		λ/nm (ε/M^{-1} cm^{-1})				
sample	solvent	Soret	Q bands			
4	DMSO	404 (84,200)	502 (7450)	531 (2680)	609 (2630)	664 (25,700)
Mal_3−TEG−Ce6	DMSO	404 (125,000)	502 (11,900)	530 (5580)	609 (5690)	665 (37,000)
Mal_3−TEG−Ce6	PBS	404 (52,300)	502 (6850)	531 (3800)	609 (3050)	664 (20,000)

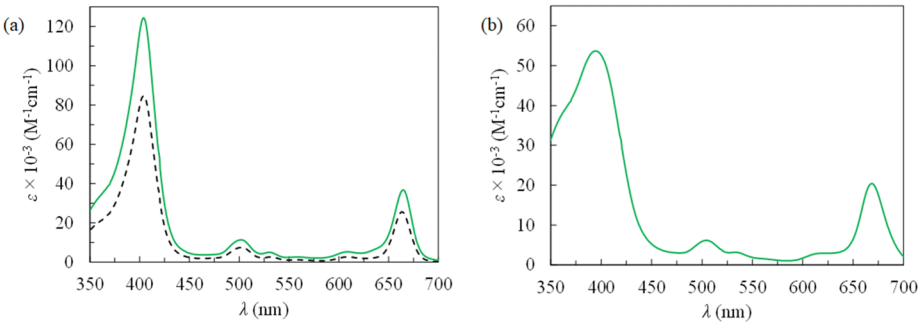

Figure 2. UV−vis spectra of (a) Mal_3−TEG−Ce6 (solid line) and **4** (dashed line) in DMSO and (b) Mal_3−TEG−Ce6 in PBS.

where $[C_{octanol}]$ and $[C_{PBS}]$ denote the concentrations of PS being portioned into the 1-octanol phase and the PBS buffer phase, respectively. The log *P* value was determined to be −0.24 for Mal_3−TEG−Ce6. We previously reported the synthesis of a fluorinated chlorin derivative that is encircled with four Mal_3 molecules (Mal_3−TFPC). Mal_3−TFPC showed a high water solubility >37 mg mL^{-1} with the log *P* of −1.78.[20] This result is simply attributable to the differences in the number of the introduced Mal_3 molecules for Mal_3−TEG−Ce6 (one Mal_3) versus Mal_3−TFPC (four Mal_3's). Consequently, the Mal_3−TEG unit is shown to be a powerful tool

https://dx.doi.org/10.1021/acsomega.0c06316
ACS Omega 2021, 6, 7023−7033

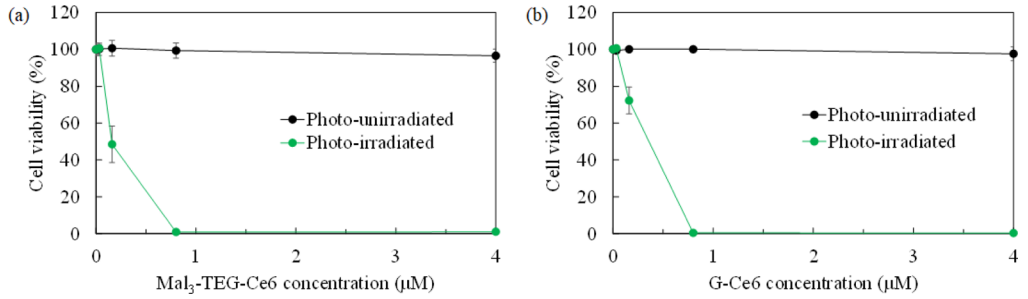

Figure 3. Photodynamic cytotoxicity of (a) Mal_3−TEG−Ce6 and (b) G−Ce6 in SNP cells. The cell viabilities are plotted as a function of the concentrations of the PSs for the photoirradiated system (671 nm) (green circles) and photounirradiated system (black circles). Each value represents the mean ± SD. (n = 6).

to make the relatively large size of a hydrophobic molecule, such as Ce6, compatible in aqueous media.

Photoabsorption Property. Table 1 summarizes the UV−vis absorption property for Mal_3−TEG−Ce6 together with that of Ce6−DME **4** as the control sample. Figure 2a displays the UV−vis spectra. In DMSO, Mal_3−TEG−Ce6 shows an absorption due to the Soret band at the maximum absorption wavelength (λ_{max}) of 404 nm with a molar absorption coefficient (ε) of 125,000 M^{-1} cm^{-1} (green solid line). Also, Mal_3−TEG−Ce6 shows an absorption due to the Q band at λ_{max} = 665 nm with ε = 37,000 M^{-1} cm^{-1}. This absorption is important for PDT in which the photochemical property can be driven by the longer wavelengths regions that is favorable for the permeability of physiological tissues. Figure 2a also shows the UV−vis spectrum of **4** as a comparison, displaying the absorptions due to the Soret band at λ_{max} = 404 nm with ε = 84,200 M^{-1} cm^{-1} and the Q band at λ_{max} = 664 nm with ε = 25,700 M^{-1} cm^{-1}. The ε values for **5** are 1.4−1.5 times higher than those of **4**. A plausible explanation is that the intermolecular associations among the Ce6 moieties are suppressed by steric hindrance due to the introduced Mal_3−TEG unit, eventually increasing the solubility of Mal_3−TEG−Ce6 in DMSO. A more noteworthy result in this study is the photochemical properties in aqueous media. Figure 2b displays the UV−vis spectrum for Mal_3−TEG−Ce6 in PBS, which exhibits absorptions due to the Soret band at λ_{max} = 404 nm with ε = 52,300 M^{-1} cm^{-1} and the Q band at λ_{max} = 664 nm with ε = 20,000 M^{-1} cm^{-1}. The λ_{max} values in PBS are consistent with those in DMSO for Mal_3−TEG−Ce6. Although the ε values in PBS are decreased as compared to those in DMSO probably due to the intermolecular associations, Mal_3−TEG−Ce6 shows photoabsorption properties derived from the Ce6 framework under the physiological conditions.

***In Vitro* PDT Test against SNP Cells.** Osaki *et al.* reported the photocytotoxicity of G−Ce6 against canine mammary carcinoma (SNP) cells.[28] The performance of G−Ce6 has been roughly estimated to be 30-fold higher than that of NPe6, a clinically approved PDT drug in Japan. Very recently, Shinoda *et al.* reported that the anticancer effect of G−Ce6 was 1000-fold higher than that of TS for the system using the human glioblastoma U251 cells.[30] Thus, the extremely high performance of G−Ce6 has already been proven. We now clarified the performance of Mal_3−TEG−Ce6 using the SNP cell system for the first time, and the result is compared to that of G−Ce6. The SNP cells were treated with different Mal_3−TEG−Ce6 concentrations (0.16, 0.80, 4.0, and 20 μM) and exposed to 671 nm red light (fluence rate = 7.3 mW/cm^2, light dose = 5 J/cm^2). Using the WST-8 assay, the cell viabilities for the photoirradiated and photounirradiated groups were measured and the ratio (%) compared to the untreated cells were determined. For the injection of G−Ce6, the use of a surfactant or organic solvent, such as DMSO, is necessary. However, Mal_3−TEG−Ce6 is a molecule that readily dissolves in water, which allows direct injection into the cell media. Figure 3a displays a plot of the cell viability as a function of the Mal_3−TEG−Ce6 concentrations. For the photounirradiated group (0 J/cm^2), no cell is killed at the Mal_3−TEG−Ce6 concentrations ranging from 0.16 to 20 μM. Hence, Mal_3 is a powerful molecular tool to introduce biocompatibility. On the other hand, for the photoirradiated group (5 J/cm^2), a very high photocytotoxicity was observed. For example, the cell viability reduces to 50% for the group using 0.16 μM Mal_3−TEG−Ce6. Furthermore, almost all the cells are killed in the group using 8.0 μM Mal_3−TEG−Ce6. Figure 3b shows the result of the G−Ce6 groups as a comparison. The half maximal (50%) inhibitory concentration (IC_{50}) values are approximately determined to be 0.26 μM for G−Ce6 and 0.15 μM for Mal_3−TEG−Ce6, indicating that Mal_3−TEG−Ce6 possesses a very high PDT activity comparable to that of G−Ce6. Thus, the availability of Mal_3 to endow both a high water solubility and high tumor cell accumulation ability to Ce6 has been proven. As for the effect of Mal_3, Nishie *et al.* has already reported that a fluorinated chlorin derivative encircled with four Mal_3 molecules (Mal_3−TFPC) exhibited a high accumulation ability to both HKN45 human gastric cancer cells and HT29 colon cancer cells.[21] We have not obtained a clear answer for the mechanism of how the Mal_3 and/or Mal_3-conjugates incorporate into the cancer cells. The facts that upregulation of glucose transporters (GLUTs) has been reported in numerous cancer types[33] suggest the possibility that the GLUTs are related to the cellar uptake for the Mal_3-system. The PDT test in the presence of the GLUT inhibitors would provide some insights into the mechanism that we would like to try in the near future.

***In Vitro* PDT Test against EMT6 Cells.** The efficacy of Mal_3−TEG−Ce6 has been confirmed using mouse mammary carcinoma (EMT6) cells. The cells were treated with diverse Mal_3−TEG−Ce6 concentrations (0.032, 0.16, 0.80, 4.0, and 20 μM) and exposed to 671 nm red light (fluence rate = 8.3 mW/cm^2). We have selected the light doses of 0, 1, 5, and 15 J/cm^2 to obtain the optimal light condition. The viabilities of EMT6 cells for the respective groups were determined after 4 h. Figure 4 displays a plot of the cell viability as a function of the Mal_3−TEG−Ce6 concentrations. Cell death is not observed for any photounirradiated groups at the Mal_3−

https://dx.doi.org/10.1021/acsomega.0c06316
ACS Omega 2021, 6, 7023−7033

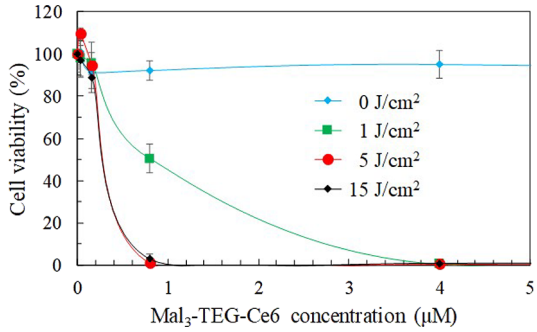

Figure 4. Photodynamic cytotoxicity of Mal_3−TEG−Ce6 in EMT6 cells (0.032, 0.16, 0.8, 4.0, and 20 μM). Each value represents the mean ± SD. (n = 6).

TEG−Ce6 concentrations ranging from 0.032 to 20 μM (0 J/cm^2). On the other hand, for the photoirradiated groups (1, 5, and 15 J/cm^2), the cells were effectively killed. Even for the group using a light dose (1 J/cm^2), the photocytotoxicity was clearly observed and almost all the cells were killed in the 4.0 μM Mal_3−TEG−Ce6 group. The cell viability is dependent on the Mal_3−TEG−Ce6 concentrations, roughly providing IC_{50} = 0.80 μM. A more significant effect is observed for the group using the increased light dose (5 J/cm^2). Cell viability reaches <5% when the Mal_3−TEG−Ce6 concentration has a low value of 0.80 μM. The tendency in the cell viability for the 15 J/cm^2 group is almost the same as that for the 5 J/cm^2 group. Consequently, the PDT using Mal_3−TEG−Ce6 induces cell death in the EMT6 cells in a manner dependent on the PS dose and the light dose.

Subcellular Localization in EMT6 Cells. Figure 5a shows fluorescence micrographs of Mal_3−TEG−Ce6 taken in EMT6

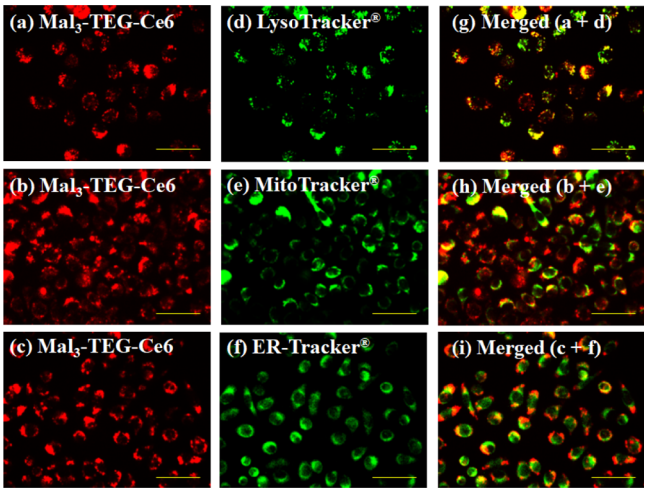

Figure 5. Subcellular localization of Mal_3−TEG−Ce6 in the EMT6 cells. The images (a−c) show the red fluorescences of Mal_3−TEG−Ce6. The images (d−f) show the green fluorescences of the probe-stained lysosome, mitochondria, and ER, respectively, which are in the same views as (a−c). The images (g−i) are the merged images of the left and middle ones. Scale bar, 50 μm.

which are stained with the lysosome, mitochondrial, and endoplasmic reticulum (ER) probes. The overlaid images have yellow-green fluorescent spots, indicating an overlap of Mal_3−TEG−Ce6 (red) and the respective probes (green). We ascertain that Mal_3−TEG−Ce6 primarily accumulates in the lysosomes. This tendency is similar to other systems with the Glc-conjugate (G−Ce6) and Mal_3−conjugate (Mal_3−TFPC). The three PSs are similar in that they are nonionic compounds.

Analysis of Annexin V (+) Cells and ROS (+) Cells. The EMT6 cells were incubated with the 0.8 μM Mal_3−TEG−Ce6 and exposed to 671 nm red light (fluence rate = 8.3 mW/cm^2, 0, 1, 5, or 15 J/cm^2). The PDT-treated cells were stained using the Apoptotic/Necrotic Cells Detection Kit (Takara Bio, Inc., Japan). Figure 6 shows an image of the resultant cells, which are divided into the following groups; control (no treatment), laser (irradiated with a light dose of 15 J/cm^2), Mal_3−TEG−Ce6 (treated with 0.8 M Mal_3−TEG−Ce6), and PDT (treated with 0.8 μM Mal_3−TEG−Ce6 and then irradiated with a light dose of 1, 5, or 15 J/cm^2). The images include the ones for the dead cells stained by ethidium homodimer III (EthD-III) (red) and annexin V-fluorescein isothiocyanate (annexin V) (green). The cells are rarely stained in the control, laser, and Mal_3−TEG−Ce6 groups, whereas a large number of cells are positively stained by EthD-III or annexin V in the PDT groups (1 and 5 J/cm^2). This indicated the occurrence of both the phosphatidylserine translocation and the loss of the plasma membrane integrity, implying that the cells are either in late apoptotic or early necrotic stages. Another result to be noted is that the number of cells is extremely low in the 15 J/cm^2 group. A possible explanation for this result is that the photocytotoxicity is so high for the 15 J/cm^2 group that the cells are destroyed and disappear.

Apoptosis has been assessed for the PDT-treated cells using the Muse Annexin V and Dead Cell Assay kit. Figure 7a shows the percentage of annexin V positive (+) cells. The apoptotic rates are 15.1, 55.0, and 42.6% for the cells in the 1, 5, and 15 J/cm^2 PDT groups, respectively. Thus, the apoptotic rates of the PDT group are clearly higher than that in the control and laser groups (all $p < 0.05$). Notably, the high apoptotic rate of 55.0% was observed in the 5 J/cm^2 group. The rate in the 15 J/cm^2 group is lower than that in the 5 J/cm^2 group. As already mentioned, there is a possibility that cells treated at 15 J/cm^2 are severely destroyed, providing inaccurate measurements as for the percentage for the annexin V (+) cells. This result suggested that the Mal_3−TEG−Ce6 PDT increased the annexin V (+) cells in a light dose-dependent manner. Finally, the generation for ROS has been assessed using the Muse Oxidative Stress kit. Figure 7b shows the percentage of the ROS positive (+) cells. A high value of 56.7% was observed for the 5 J/cm^2 group. The percentage of ROS positive (+) cells of the 5 J/cm^2 PDT group was significantly higher than that for the laser group ($p < 0.05$). The percentage of ROS (+) cells fairly agrees with that of the annexin V (+) cells, suggesting that apoptosis of the EMT6 cells is due to the ROS generated as a result of the photoirradiation of Mal_3−TEG−Ce6 in the presence of molecular oxygen.

■ CONCLUSIONS

Mal_3, an oligosaccharide in which three glucose molecules are coupled together, has been conjugated to Ce6 by using two additional molecular tools such as PA and the TEG derivative. This allowed the production of the Mal_3−Ce6 conjugate linked *via* the TEG-spacer, Mal_3−TEG−Ce6. A remarkable result is that Mal_3−TEG−Ce6 acquires water solubility, while its original photoabsorption properties due to Ce6 remain intact even in physiological media, which has not been achieved by the monosaccharide conjugation. *In vitro* tests against SNP cells have indicated that Mal_3−TEG−Ce6 possesses an

https://dx.doi.org/10.1021/acsomega.0c06316
ACS Omega 2021, 6, 7023−7033

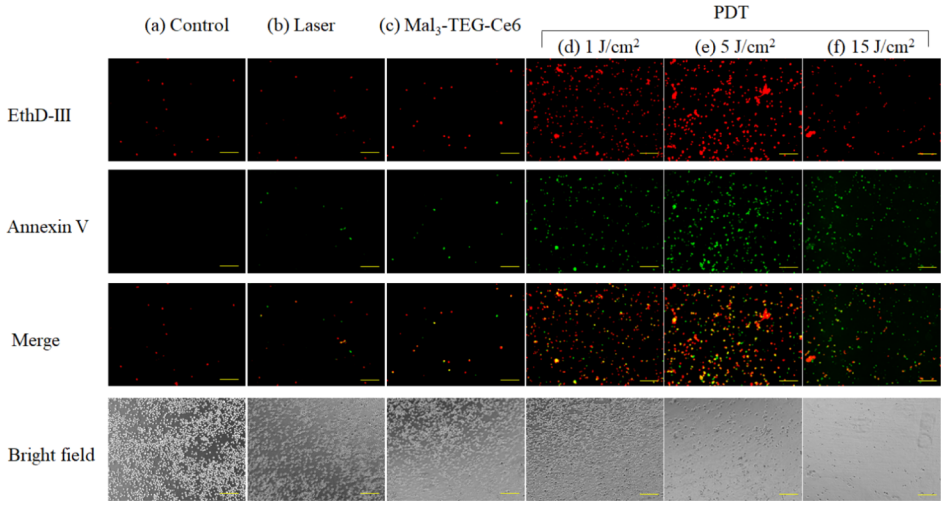

Figure 6. Representative images of EMT6 cells stained with EthD-III (red) and annexin V (green) for the PDT groups using the conditions of the Mal_3−TEG−Ce6 concentration and the light dose of (a) 0 μM and 0 J/cm^2, (b) 0 μM and 15 J/cm^2, (c) 0.8 μM and 0 J/cm^2, (d) 0.8 μM and 1 J/cm^2, (e) 0.8 μM and 5 J/cm^2, and (f) 0.8 μM and 15 J/cm^2, respectively. Scale bar, 500 μm.

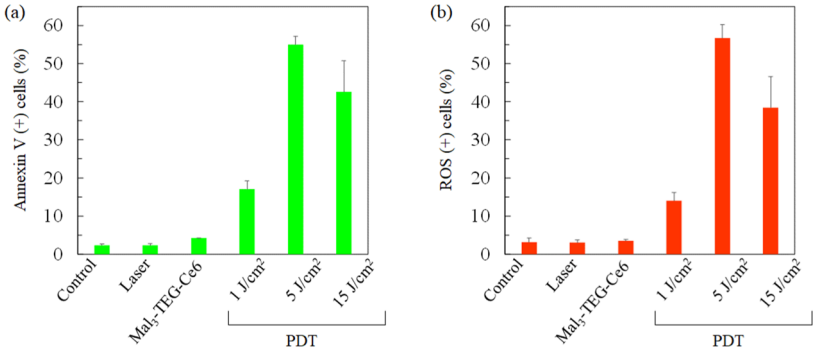

Figure 7. Percentages of (a) annexin V (+) cells and (b) ROS (+) cells. Data were analyzed using Dunn's multiple comparison test [(a) *p < 0.05; control *vs* 5 J/cm^2, laser *vs* 5 J/cm^2 and (b) *p < 0.05; laser *vs* 5 J/cm^2]. The results are presented as the mean ± standard deviation.

extremely high PDT activity comparable to that of the previously reported monosaccharide-based PS such as G−Ce6. *In vitro* tests against EMT6 cells provided further insights into the Mal_3−TEG−Ce6 PDT system that includes both apoptosis and necrosis of the EMT6 cells is due to the ROS generated as a result of the photochemical reaction between Mal_3−TEG−Ce6 and tissue molecular oxygen. We have experimentally proven that Mal_3−TEG−Ce6 has a high potential as an advanced PS showing the currently desired properties.

EXPERIMENTAL SECTION

Materials. N_3−TEG−OTs **2**[32] and chlorin e6−DME **4**[34] were prepared according to the literature. Mal_3 (Sigma-Aldrich, >90%), PA (Tokyo Chemical Industry Co., Japan, >95.0%), $CuSO_4$ (Wako Pure Chemical Industries, Japan, 97.5%), sodium L-ascorbate (Wako Pure Chemical Industries, Japan, 98.0%), Cs_2CO_3 (Tokyo Chemical Industry Co., Japan, >98%), *tert*-butyl alcohol (Tokyo Chemical Industry Co., Japan, >99.0%), and dry *N*,*N*-dimethylformamide (Wako Pure Chemical Industries, Japan, 99.5%) were used as received. All other materials were obtained from commercial sources and used as received, unless otherwise stated.

Instruments. The ^{1}H and ^{13}C NMR spectra were recorded using JEOL JNM-ECX400 and JNM-ECZ600R instruments. The infrared (IR) spectra were recorded using a Horiba FT-720 spectrometer. The UV−vis spectra were recorded by a JASCO V-500 spectrophotometer. The high-resolution mass spectra were recorded by a JEOL AccuTOF JMS-T100LC (ESI-MS). Aqueous preparative size-exclusion chromatography (SEC) was performed using ChromNAV software, a JASCO LC-NetII/ADC interface box, a JASCO FC-2088-30 fraction collector controller, a JASCO PU-2086 Plus pump, a JASCO UV-2075 Plus detector, an Advantec CHF 122 SC fraction collector, and a Shodex OH pak SB-2002.5 column (20 × 300 mm, average bead size: 10 μm, exclusion limit: 1 × 10^4) using water as the eluent at a flow rate of 2.5 mL min^{-1} and room temperature.

Synthesis. *N-Acetyl-N-ethynyl-[(O-α-D-glucopyranosyl)-(1 → 4)]$_2$-β-D-glucopyranoside (Mal_3−Alkyne **1**).* The synthesis of Mal_3−alkyne **1** has already been reported elsewhere.[35] The mixture of Mal_3 (500 mg, 991 μmol) and PA (900 μL, 14.1 mmol) was stirred at room temperature. The consumption of Mal_3 was monitored by TLC (silica gel 60 F_{254}, CH_3CN/H_2O = 2:1). After 72 h, dry MeOH (1.00 mL) was added and the mixture was poured into dry CH_2Cl_2 (150 mL). The formed precipitates were collected by filtration using a 1.0 μm pore-sized PTFE membrane filter and washed with a mixture of 1:3 dry MeOH/dry CH_2Cl_2 (8.00 mL). A solution of Ac_2O (3.56 g, 34.9 mmol) in dry MeOH (66.0 mL) was added to the obtained solid, and the resulting mixture was stirred overnight at room temperature and then evaporated. A

https://dx.doi.org/10.1021/acsomega.0c06316
ACS Omega 2021, 6, 7023−7033

mixture of 1:1 MeOH/toluene (10.0 mL) was added, and the mixture was evaporated. This procedure was repeated until Ac_2O and acetic acid were removed from the mixture. The residue was redissolved in H_2O (5 mL) and freeze-dried to give the target **1** as a white solid (360 mg, 62.2%). R_f = 0.53 (CH_3CN/H_2O = 2/1).

2-(2-(2-(2-[[(4-Methylphenyl)sulfonyl]oxy]ethoxy)ethoxy)-ethoxy)ethyl-1H-1,2,3-triazol-1-yl-methyl O-(α-D-glucopyranosyl)-(1 → 4)-(α-D-glucopyranosyl)-(1 → 4)-N-acetyl-N-β-D-glucopyranoside (Mal_3−TEG−OTs ***3****).* A mixture of Mal_3−alkyne **1** (193 mg, 331 μmol) and N_3−TEG−OTs **2** (124 mg, 331 μmol) was stirred in a mixture of 1:1 *tert*-butyl alcohol/H_2O (33.0 mL). $CuSO_4$ (52.8 mg, 331 μmol) and sodium L-ascorbate (197 mg, 993 μmol) were added to the mixture, which was stirred at room temperature. After 24 h, the mixture was evaporated to dryness and the residue was purified by aqueous preparative SEC. The target product was redissolved in H_2O (5.00 mL) and freeze-dried to give **3** as a white solid (126 mg, 39.7%). R_f = 0.33 ($CHCl_3/CH_3OH$ = 3/1). ^{1}H NMR (400 MHz, D_2O): δ (ppm) = 8.00 and 7.77 (1H, 2 × s, minor and major rotamers, respectively, =C*H*N), 7.67 (2H, d, *J* = 8.2 Hz, Ar*H*), 7.32 (2H, d, *J* = 8.2 Hz, Ar*H*), 5.45 and 4.97 (1H, 2 × d, minor and major rotamers, *J* = 9.1 Hz and *J* = 8.2 Hz, respectively, *H*-1^{Mal1}), 5.25−5.21 (2H, m, *H*-1$^{Mal2-Mal3}$), 4.45 (2H, s, N(COCH$_3$)C*H*$_2$), 4.40 (2H, t, *J* = 10 Hz, NC*H*$_2$), 4.11 (2H, t, *J* = 8.6 Hz, C*H*$_2$OTs), 3.83−3.24 (30H, m, *H*-2$^{Mal1-Mal3}$, *H*-3$^{Mal1-Mal3}$, *H*-4$^{Mal1-Mal3}$, *H*-5$^{Mal1-Mal3}$, *H*-6$^{Mal1-Mal3}$, NCH$_2$C*H*$_2$(OC*H*$_2$C*H*$_2$)$_2$OC*H*$_2$CH$_2$OTs), 2.28 (3H, s, ArC*H*$_3$), 2.08 and 1,95 (3H, 2 × s, major and minor rotamers, respectively, NCOC*H*$_3$). ^{13}C NMR (100 MHz, D_2O): δ (ppm) = 174.9 (COCH$_3$), 146.5 (Ar), 146.5 (NC=CHN), 130.9 (Ar), 130.2 (Ar), 127.8 (Ar), 124.9 (NC=CHN), 100.0 (*C*-1$^{Mal2-Mal3}$), 87.0 (*C*-1^{Mal1}), 76.6, 73.4, 72.7, 71.8, 71.5, 71.2 (*C*-2$^{Mal1-Mal3}$, *C*-3$^{Mal1-Mal3}$, *C*-4$^{Mal1-Mal3}$, *C*-5$^{Mal1-Mal3}$), 70.2, 70.1, 69.7, 69.5, 69.3, 68.8, 68.0 (NCH$_2$CH$_2$O, OCH$_2$CH$_2$O), 60.6 (*C*-6$^{Mal1-Mal3}$), 50.1 (N(COCH$_3$)CH$_2$), 21.2 (ArCH$_3$), 20.9 (NCOCH$_3$). FT-IR (KBr): ν (cm^{-1}) 3394, 2923, 1732, 1450, 1356, 1034, 924, 816, 771, 698, 561. HR-ESI-MS: [M + Na]$^+$ ion peak at *m*/*z* 979.33019 corresponding to $C_{38}H_{60}N_4O_{22}SNa$ (calcd. 979.33176).

13^1-(2-(2-(2-(2-[1H-1,2,3-Triazol-1-yl-methyl-O-(α-D-glucopyranosyl)-(1 → 4)-(α-D-glucopyranosyl)-(1 → 4)-N-acetyl-N-β-D-glucopyranosyl]ethoxy)ethoxy)ethoxy)-ethoxycarbonyl) Chlorin e6 Dimethyl Ester (Mal_3−TEG−Ce6). The mixture of Mal_3−TEG−OTs **3** (23.8 mg, 24.9 μmol), chlorin e6-DME **4** (15.6 mg, 24.9 μmol), and Cs_2CO_3 (8.10 mg, 24.9 μmol) in dry *N*,*N*-dimethylformamide (500 μL) was stirred at room temperature for 48 h. The mixture was evaporated to dryness, and the residue was purified by silica gel column chromatography ($CHCl_3$/MeOH = 4/1 R_f = 0.11) to give the target Mal_3−TEG−Ce6 as a green solid (22.1 mg, 63.1%). Data for Mal_3−TEG−Ce6: R_f = 0.32 ($CHCl_3/CH_3OH$ = 3/1). ^{1}H NMR (600 MHz, DMSO-d_6): δ (ppm) = 9.78 (1H, s, H_{chl}-10), 9.67 (1H, s, H_{chl}-5), 9.07 (1H, s, H_{chl}-20), 8.29 (1H, dd, *J* = 11, *J* = 12 Hz, H_{chl}-3^1), 8.01 and 7.85 (1H, 2 × s, minor and major rotamers, respectively, =C*H*N), 6.46 and 6.20 (2H, d, *J* = 19 and 12 Hz, respectively, H_{chl}-3^2), 5.46 and 4.85 (1H, 2 × d, minor and major rotamers, *J* = 4.8 Hz and *J* = 9.0 Hz, respectively, *H*-1^{Mal1}), 5.31 (1H, br, H_{chl}-15^1), 5.03−5.00 (2H, m, *H*-1$^{Mal2-Mal3}$), 4.80−4.74 (1H, m, C*H*$_2$OC=O), 4.60−4.56 (1H, m, H_{chl}-18), 4.56−4.53 (2H, m, N(COCH$_3$)C*H*$_2$), 4.45 (1H, m, H_{chl}-17), 4.45−4.38 (2H, m, NC*H*$_2$CH$_2$), 3.97 (2H, t, *J* = 12 Hz, OC*H*$_2$CH$_2$OC=O), 3.81−3.77 (2H, q, H_{chl}-8^1), 3.75−3.06 (44H, m, *H*-2$^{Mal1-Mal3}$, *H*-3$^{Mal1-Mal3}$, *H*-4$^{Mal1-Mal3}$, *H*-5$^{Mal1-Mal3}$, *H*-6$^{Mal1-Mal3}$, NCH$_2$CH$_2$(OCH$_2$CH$_2$)$_2$O, H_{chl}-2^1, H_{chl}-7^1, H_{chl}-12^1, H_{chl}-15^4, H_{chl}-17^5), 2.70 and 2.09 (1H, m, H_{chl}-17^2), 2.39 and 1.59 (1H, m, H_{chl}-17^1), 2.07 and 1.93 (3H, 2 × s, major and minor rotamers, respectively, NCOC*H*$_3$), 1.65−1.67 (6H, m, H_{chl}-8^2, H_{chl}-18^1), −1.50 (1H, s, H_{chl}-21), −1.70 (1H, s, H_{chl}-23). ^{13}C NMR (150 MHz, DMSO-d_6): δ (ppm) = 173.8 (C_{chl}-15^2), 173.1 (C_{chl}-17^3), 171.3 (NCOCH$_3$), 171.1 (C_{chl}-13^1), 168.7 (C_{chl}-19), 168.1 (C_{chl}-16), 154.6 (C_{chl}-6), 148.8 (C_{chl}-9), 145.5 (C_{chl}-8) 145.4 (NC=CHN), 139.4 (C_{chl}-2), 136.7 (C_{chl}-4), 136.5 (C_{chl}-7), 135.3 (C_{chl}-12), 134.9 (C_{chl}-14), 134.7 (C_{chl}-3), 131.4 (C_{chl}-1, C_{chl}-11), 129.6 (C_{chl}-3^1), 129.0 (C_{chl}-13), 124.3 (NC=CHN), 122.8 (C_{chl}-3^2), 102.9 (C_{chl}-15), 102.5 (C_{chl}-10), 101.4 (*C*-1^{Mal2,3}), 98.8 (C_{chl}-5), 94.7 (C_{chl}-20), 87.4 (*C*-1^{Mal1}), 80.1, 74.0, 73.8, 73.1, 72.5, 72.3 (*C*-2^{Mal1-3}, *C*-3^{Mal1-3}, *C*-4^{Mal1-3}, *C*-5^{Mal1-3}), 70.7, 70.3, 70.2, 70.1, 69.1, 68.9, 65.6 (NCH$_2$CH$_2$O, OCH$_2$CH$_2$O), 61.3 (*C*-6^{Mal1-3}), 52.9 (C_{chl}-17), 52.5 (C_{chl}-15^4), 51.9 (C_{chl}-17^5), 49.8 (N(COCH$_3$)CH$_2$), 48.7 (C_{chl}-18), 38.1 (C_{chl}-15^1), 31.0 (C_{chl}-17^2), 29.9 (C_{chl}-17^1), 23.3 (C_{chl}-18^1), 22.3 (NCOCH$_3$), 19.3 (C_{chl}-8^1), 18.3 (C_{chl}-8^2), 12.5 (C_{chl}-2^1), 12.3 (C_{chl}-12^1), 11.4 (C_{chl}-7^1). FT-IR (KBr): ν (cm^{-1}) 3411, 2922, 2868, 2571, 1795, 1723, 1643, 1539, 1437, 1344, 1147, 1066, 1030, 843, 798, 766, 723, 620. HR-ESI-MS: [M + Na]$^+$ ion peak at *m*/*z* 1431.60547 corresponding to $C_{67}H_{92}N_8O_{25}Na$ (calcd. 1431.60713). UV−vis (*c* 10.0 μM, DMSO, path length = 1 cm, 25 °C): λ/nm (ε × 10^{-3}/M^{-1} cm^{-1}) = 404 (124), 502 (11.3), 530 (4.98), 609 (5.23), 665 (36.7).

Cell Culture. Canine mammary carcinoma (SNP) cells were established by the author.[36] The mouse mammary carcinoma (EMT6) cells were supplied by Professor Yoshihiro Uto of Tokushima University (Tokushima, Japan). The SNP and EMT6 cells were cultured in a 250 mL tissue culture flask (Corning Incorporated, Corning, NY, USA) containing RPMI 1640 medium (Invitrogen; Thermo Fisher Scientific, Inc., Waltham, MA, USA) supplemented with 10% heat-inactivated fetal bovine serum (Nichirei Biosciences, Tokyo, Japan) and PSN (5 mg/mL penicillin, 5 mg/mL streptomycin, and 10 mg/mL neomycin) solution (Invitrogen), then incubated in 5% CO_2 at 37 °C. The cells were washed with phosphate-buffered saline for subculturing and then harvested from near-confluent cultures *via* a brief exposure to a solution containing 0.25% trypsin and 1 mmol/L tetrasodium ethylenediaminetetraacetic acid with phenol red (Invitrogen). Trypsinization was terminated using RPMI 1640 medium containing 10% fetal bovine serum. The trypsinized cells were transferred to a new tissue culture flask.

In Vitro **PDT Test.** We seeded 1 × 10^4 SNP cells or EMT6 cells into each well of 96-well plates (Corning, Inc., New York, NY, USA) followed by overnight incubation. The cells were then incubated with various Mal_3−TEG−Ce6 concentrations for 24 h at 37 °C. After washing with fresh media, the cells were irradiated with 671 nm light emitted by a semiconductor laser (Osada Electric Co., Ltd., Tokyo, Japan), using an optical fiber with a microlens delivery attachment (Pioneer Optics, Inc., Windsor Lock, CT, USA). PDT was performed at 7.3 mW/cm^2 in cells exposed to four concentrations of Mal_3−TEG−Ce6 (0, 0.16, 0.8, 4, and 20 μM) using a light dose of 5 J/cm^2. The cells were then incubated for 24 h in the dark prior to examining the cell viability using the Cell Counting Kit-8 (Dojindo, Kumamoto, Japan) according to the manufacturer's instructions.

https://dx.doi.org/10.1021/acsomega.0c06316
ACS Omega 2021, 6, 7023−7033

Subcellular Localization. We cultured 1 × 10^5 EMT6 cells in a 35-mm Petri dish (Thermo Fisher Scientific, Waltham, MA, USA). The EMT6 cells were then incubated with Mal_3−TEG−Ce6 at a final concentration of 20 μM in complete cell culture medium for 6 h, followed by coincubation with 50 nM LysoTracker Yellow HCK-123 (Invitrogen), 50 nM MitoTracker Green FM (Invitrogen), and 50 nM ER-Tracker Green (Invitrogen) and for an additional 30 min at 23 °C in the culture medium before fluorescence microscopy. The fluorescence of Mal_3−TEG−Ce6 was detected with a filter (excitation, 405 nm; emission, 640 nm) using an all-in-one fluorescence microscope (BZ-X800, Keyence Co., Osaka, Japan). A BZ-X filter GFP (excitation, 470 nm; emission, 525 nm) was used to observe the mitochondria and lysosome; the green and red images were combined to form an overlay image.

Analysis of Apoptosis and ROS. The EMT6 cells were seeded at a density of 1.0 × 10^5 cells/well in 35 mm Petri dishes containing 2 mL of culture medium. Following 24 h of incubation, the cells were divided into the following groups: control (no treatment); laser (irradiated with a light dose of 15 J/cm^2); Mal_3−TEG−Ce6 (treated with 0.8 M Mal_3−TEG−Ce6); and PDT (treated with 0.8 μM Mal_3−TEG−Ce6 and then irradiated with a light dose of 1, 5, or 15 J/cm^2). The cells were incubated with 0.8 μM Mal_3−TEG−Ce6 for 4 h. After washing with fresh media, the cells were irradiated by a 671 nm laser light (8.3 mW/cm^2; 1, 5, and 15 J/cm^2) emitted by a DPPS laser (HangZhou NaKu Technology Co., Ltd., China, Zhejiang) using an optical fiber with a microlens delivery attachment. Apoptosis was assessed 4 h after the laser irradiation using the Muse Annexin V and Dead Cell Assay Kit (Merk Millipore, Germany) according to the manufacturer's protocols. Annexin V was used to detect phosphatidylserine on the external membrane of the apoptotic cells. The ROS generation was assessed 4 h after laser irradiation using the Muse Oxidative Stress Kit (Merk Millipore, Germany) according to the manufacturer's protocols; this kit determines the percentage of cells that are negative (healthy cells) and positive for ROS (cells containing ROS). Single-cell suspensions were then loaded onto the Muse Cell Analyzer (EMD Millipore Co.).

■ ASSOCIATED CONTENT

Supporting Information

The Supporting Information is available free of charge at https://pubs.acs.org/doi/10.1021/acsomega.0c06316.

IR spectra of **2**, **3**, and Mal_3−TEG−Ce6 and the ^{13}C NMR spectra of **3** and Mal_3−TEG−Ce6 (PDF)

■ AUTHOR INFORMATION

Corresponding Authors

Atsushi Narumi − *Graduate School of Organic Materials Science, Yamagata University, Yonezawa 992-8510, Japan;* orcid.org/0000-0002-8968-9574; Email: narumi@yz.yamagata-u.ac.jp

Tomohiro Osaki − *Joint Department of Veterinary Clinical Medicine, Faculty of Agriculture, Tottori University, Tottori 680-8553, Japan*; Email: tosaki@tottori-u.ac.jp

Authors

Rioko Rachi − *Graduate School of Organic Materials Science, Yamagata University, Yonezawa 992-8510, Japan*

Hiromi Yamazaki − *Graduate School of Organic Materials Science, Yamagata University, Yonezawa 992-8510, Japan*

Seigou Kawaguchi − *Graduate School of Organic Materials Science, Yamagata University, Yonezawa 992-8510, Japan;* orcid.org/0000-0002-5283-781X

Moriya Kikuchi − *Faculty of Engineering, Yamagata University, Yonezawa 992-8510, Japan*

Hiroyuki Konno − *Graduate School of Science and Engineering, Yamagata University, Yonezawa, Yamagata 992-8510, Japan;* orcid.org/0000-0002-6629-6102

Yoshiharu Okamoto − *Joint Department of Veterinary Clinical Medicine, Faculty of Agriculture, Tottori University, Tottori 680-8553, Japan*

Xiande Shen − *Research Center for Polymer Materials, School of Materials Science and Engineering, Changchun University of Science and Technology, Jilin 130022, China*

Toyoji Kakuchi − *Research Center for Polymer Materials, School of Materials Science and Engineering, Changchun University of Science and Technology, Jilin 130022, China;* orcid.org/0000-0001-9668-1442

Hiromi Kataoka − *Department of Gastroenterology and Metabolism, Nagoya City University Graduate School of Medical Sciences, Nagoya 467-8601, Japan*

Akihiro Nomoto − *Department of Applied Chemistry, Graduate School of Engineering, Osaka Prefecture University, Sakai, Osaka 599-8531, Japan*

Tomokazu Yoshimura − *KYOUSEI Science Center for Life and Nature, Nara Women's University, Nara 630-8506, Japan;* orcid.org/0000-0001-8283-1032

Shigenobu Yano − *KYOUSEI Science Center for Life and Nature, Nara Women's University, Nara 630-8506, Japan*

Complete contact information is available at: https://pubs.acs.org/10.1021/acsomega.0c06316

Author Contributions

The manuscript was written through contributions of all the authors. All the authors have given approval to the final version of the manuscript.

Funding

This research was partly supported by JSPS KAKENHI grant numbers 25288028 and 18K05161.

Notes

The authors declare no competing financial interest.

■ ACKNOWLEDGMENTS

The author thanks the Yamagata University YU-COE(C) project.

■ REFERENCES

(1) Yano, S.; Hirohara, S.; Obata, M.; Hagiya, Y.; Ogura, S.-i.; Ikeda, A.; Kataoka, H.; Tanaka, M.; Joh, T. Current States and Future Views in Photodynamic Therapy. *J. Photochem. Photobiol., C* **2011**, *12*, 46−67.

(2) Ethirajan, M.; Chen, Y.; Joshi, P.; Pandey, R. K. The Role of Porphyrin Chemistry in Tumor Imaging and Photodynamic Therapy. *Chem. Soc. Rev.* **2011**, *40*, 340−362.

(3) Singh, S.; Aggarwal, A.; Bhupathiraju, N. V. S. D. K.; Arianna, G.; Tiwari, K.; Drain, C. M. Glycosylated Porphyrins, Phthalocyanines, and Other Porphyrinoids for Diagnostics and Therapeutics. *Chem. Rev.* **2015**, *115*, 10261−10306.

(4) Bhupathiraju, N. V. S. D. K.; Rizvi, W.; Batteas, J. D.; Drain, C. M. Fluorinated Porphyrinoids as Efficient Platforms for New

Photonic Materials, Sensors, and Therapeutics. *Org. Biomol. Chem.* **2016**, *14*, 389−408.
(5) Bonnett, R.; White, R. D.; Winfield, U. J.; Berenbaum, M. C. Hydroporphyrins of the Meso-Tetra(Hydroxyphenyl)Porphyrin Series as Tumor Photosensitizers. *Biochem. J.* **1989**, *261*, 277−280.
(6) Spikes, J. D.; Bommer, J. C. Photosensitizing Properties of Mono-L-Aspartyl Chlorin e6 (NPe6) - a Candidate Sensitizer for the Photodynamic Therapy of Tumors. *J. Photochem. Photobiol., B* **1993**, *17*, 135−143.
(7) Chen, Y.; Zheng, X.; Dobhal, M. P.; Gryshuk, A.; Morgan, J.; Dougherty, T. J.; Oseroff, A.; Pandey, R. K. Methyl Pyropheophorbide-a Analogues: Potential Fluorescent Probes for the Peripheral-Type Benzodiazepine Receptor. Effect of Central Metal in Photosensitizing Efficacy. *J. Med. Chem.* **2005**, *48*, 3692−3695.
(8) Sol, V.; Blais, J. C.; Bolbach, G.; Carré, V.; Granet, R.; Guilloton, M.; Spiro, M.; Krausz, P. Toward Glycosylated Peptidic Porphyrins: a New Strategy for PDT? *Tetrahedron Lett.* **1997**, *38*, 6391−6394.
(9) Maillard, P.; Hery, C.; Momenteau, M. Synthesis, Characterization and Photocytotoxicity of a Glycoconjugated meso-Monoarylbenzochlorin. *Tetrahedron Lett.* **1997**, *38*, 3731−3734.
(10) Mikata, Y.; Onchi, Y.; Shibata, M.; Kakuchi, T.; Ono, H.; Ogura, S.-i.; Okura, I.; Yano, S. Synthesis and Phototoxic Property of tetra- and octa-Glycoconjugated Tetraphenylchlorins. *Bioorg. Med. Chem. Lett.* **1998**, *8*, 3543−3548.
(11) Sol, V.; Blais, J. C.; Carré, V.; Granet, R.; Guilloton, M.; Spiro, M.; Krausz, P. Synthesis, Spectroscopy, and Photocytotoxicity of Glycosylated Amino Acid Porphyrin Derivatives as Promising Molecules for Cancer Phototherapy. *J. Org. Chem.* **1999**, *64*, 4431−4444.
(12) Silva, A. M. G.; Tomé, A. C.; Neves, M. G. P. M. S.; Silva, A. M. S.; Cavaleiro, J. A. S.; Perrone, D.; Dondoni, A. Porphyrins in 1,3-Dipolar Cycloaddition Reactions with Sugar Nitrones. Synthesis of Glycoconjugated Isoxazolidine-Fused Chlorins and Bacteriochlorins. *Tetrahedron Lett.* **2002**, *43*, 603−605.
(13) Hirohara, S.; Obata, M.; Alitomo, H.; Sharyo, K.; Ogata, S.-i.; Ohtsuki, C.; Yano, S.; Ando, T.; Tanihara, M. Structure-Photodynamic Effect Relationships of 24 Glycoconjugated Photosensitizers in HeLa Cells. *Biol. Pharm. Bull.* **2008**, *31*, 2265−2272.
(14) Hirohara, S.; Obata, M.; Alitomo, H.; Sharyo, K.; Ando, T.; Tanihara, M.; Yano, S. Synthesis, Photophysical Properties and Sugar-Dependent in Vitro Photocytotoxicity of Pyrrolidine-Fused Chlorins bearing S-Glycosides. *J. Photochem. Photobiol., B* **2009**, *97*, 22−33.
(15) Singh, S.; Aggarwal, A.; Thompson, S.; Tomé, J. P. C.; Zhu, X.; Samaroo, D.; Vinodu, M.; Gao, R.; Drain, C. M. Synthesis and Photophysical Properties of Thioglycosylated Chlorins, Isobacteriochlorins, and Bacteriochlorins for Bioimaging and Diagnostics. *Bioconjugate Chem.* **2010**, *21*, 2136−2146.
(16) Tanaka, M.; Kataoka, H.; Mabuchi, M.; Sakuma, S.; Takahashi, S.; Tujii, R.; Akashi, H.; Ohi, H.; Yano, S.; Morita, A.; Joh, T. Anticancer Effects of Novel Photodynamic Therapy with Glycoconjugated Chlorin for Gastric and Colon Cancer. *Anticancer Res.* **2011**, *31*, 763.
(17) Aggarwal, A.; Thompson, S.; Singh, S.; Newton, B.; Moore, A.; Gao, R.; Gu, X.; Mukherjee, S.; Drain, C. M. Photophysics of Glycosylated Derivatives of a Chlorin, Isobacteriochlorin and Bacteriochlorin for Photodynamic Theragnostics: Discovery of a Two-photon-absorbing Photosensitizer. *Photochem. Photobiol.* **2014**, *90*, 419−430.
(18) Tanaka, M.; Kataoka, H.; Yano, S.; Ohi, H.; Moriwaki, K.; Akashi, H.; Taguchi, T.; Hayashi, N.; Hamano, S.; Mori, Y.; Kubota, E.; Tanida, S.; Joh, T. Antitumor Effects in Gastrointestinal Stromal Tumors Using Photodynamic Therapy with a Novel Glucose-Conjugated Chlorin. *Mol. Cancer Ther.* **2014**, *13*, 767−775.
(19) Hayashi, N.; Kataoka, H.; Yano, S.; Tanaka, M.; Moriwaki, K.; Akashi, H.; Suzuki, S.; Mori, Y.; Kubota, E.; Tanida, S.; Takahashi, S.; Joh, T. A Novel Photodynamic Therapy Targeting Cancer Cells and Tumor-Associated Macrophages. *Mol. Cancer Ther.* **2015**, *14*, 452−460.
(20) Narumi, A.; Tsuji, T.; Shinohara, K.; Yamazaki, H.; Kikuchi, M.; Kawaguchi, S.; Mae, T.; Ikeda, A.; Sakai, Y.; Kataoka, H.; Inoue, M.; Nomoto, A.; Kikuchi, J.-i.; Yano, S. Maltotriose-Conjugation to a Fluorinated Chlorin Derivative Generating a PDT Photosensitizer with Improved Water-Solubility. *Org. Biomol. Chem.* **2016**, *14*, 3608−3613.
(21) Nishie, H.; Kataoka, H.; Yano, S.; Kikuchi, J.-i.; Hayashi, N.; Narumi, A.; Nomoto, A.; Kubota, E.; Joh, T. A Next-Generation Bifunctional Photosensitizer with Improved Water-Solubility for Photodynamic Therapy and Diagnosis. *Oncotarget* **2016**, *7*, 74259−74268.
(22) Shinoda, Y.; Takahashi, T.; Akimoto, J.; Ichikawa, M.; Yamazaki, H.; Narumi, A.; Yano, S.; Fujiwara, Y. Comparative Photodynamic Therapy Cytotoxicity of Mannose-Conjugated Chlorin and Talaporfin Sodium in Cultured Human and Rat Cells. *J. Toxicol. Sci.* **2017**, *42*, 111−119.
(23) Warburg, O. On the Origin of Cancer Cells. *Science* **1956**, *123*, 309−314.
(24) Zheng, G.; Graham, A.; Shibata, M.; Missert, J. R.; Oseroff, A. R.; Dougherty, T. J.; Pandey, R. K. Synthesis of β-Galactose-Conjugated Chlorins Derived by Enyne Metathesis as Galectin-Specific Photosensitizers for Photodynamic Therapy. *J. Org. Chem.* **2001**, *66*, 8709−8716.
(25) Zhang, M.; Zhang, Z.; Blessington, D.; Li, H.; Busch, T. M.; Madrak, V.; Miles, J.; Chance, B.; Glickson, J. D.; Zheng, G. Pyropheophorbide 2-Deoxyglucosamide: A New Photosensitizer Targeting Glucose Transporters. *Bioconjugate Chem.* **2003**, *14*, 709−714.
(26) Cieckiewicz, E.; Mathieu, V.; Angenot, L.; Gras, T.; Dejaegher, B.; de Tullio, P.; Pirotte, B.; Frédérich, M. Semisynthesis and in Vitro Photodynamic Activity Evaluations of Halogenated and Glycosylated Derivatives of Pheophorbide a. *Eur. J. Org. Chem.* **2015**, *2015*, 6061−6074.
(27) Nishie, H.; Kataoka, H.; Yano, S.; Yamaguchi, H.; Nomoto, A.; Tanaka, M.; Kato, A.; Shimura, T.; Mizoshita, T.; Kubota, E.; Tanida, S.; Joh, T. Excellent Antitumor Effects for Gastrointestinal Cancers Using Photodynamic Therapy with a Novel Glucose Conjugated Chlorin e6. *Biochem. Biophys. Res. Commun.* **2018**, *496*, 1204−1209.
(28) Osaki, T.; Hibino, S.; Yokoe, I.; Yamaguchi, H.; Nomoto, A.; Yano, S.; Mikata, Y.; Tanaka, M.; Kataoka, H.; Okamoto, Y. A Basic Study of Photodynamic Therapy with Glucose-Conjugated Chlorin e6 Using Mammary Carcinoma Xenografts. *Cancers* **2019**, *11*, 636.
(29) Otvagin, V. F.; Kuzmina, N. S.; Krylova, L. V.; Volovetsky, A. B.; Nyuchev, A. V.; Gavryushin, A. E.; Meshkov, I. N.; Gorbunova, Y. G.; Romanenko, Y. V.; Koifman, O. I.; Balalaeva, I. V.; Fedorov, A. Y. Water-Soluble Chlorin/Arylaminoquinazoline Conjugate for Photodynamic and Targeted Therapy. *J. Med. Chem.* **2019**, *62*, 11182−11193.
(30) Shinoda, Y.; Kujirai, K.; Aoki, K.; Morita, M.; Masuda, M.; Zhang, L.; Kaixin, Z.; Nomoto, A.; Takahashi, T.; Tsuneoka, Y.; Akimoto, J.; Kataoka, H.; Rachi, R.; Narumi, A.; Yoshimura, T.; Yano, S.; Fujiwara, Y. Novel Photosensitizer β-Mannose-Conjugated Chlorin e6 as a Potent Anticancer Agent for Human Glioblastoma U251 Cells. *Pharmaceuticals* **2020**, *13*, 316.
(31) Togashi, D.; Otsuka, I.; Borsali, R.; Takeda, K.; Enomoto, K.; Kawaguchi, S.; Narumi, A. Maltopentaose-Conjugated CTA for RAFT Polymerization Generating Nanostructured Bioresource-Block Copolymer. *Biomacromolecules* **2014**, *15*, 4509−4519.
(32) Yue, X.; Feng, Y.; Yu, Y. B. Synthesis and Characterization of Fluorinated Conjugates of Albumin. *J. Fluorine Chem.* **2013**, *152*, 173−181.
(33) Ancey, P. B.; Contat, C.; Meylan, E. Glucose Transporters in Cancer - from Tumor Cells to the Tumor Microenvironment. *FEBS J.* **2018**, *285*, 2926−2943.
(34) Jinadasa, R. G. W.; Hu, X.; Vicente, M. G. H.; Smith, K. M. Syntheses and Cellular Investigations of 17^3-, 15^2-, and 13^1-Amino Acid Derivatives of Chlorin e6. *J. Med. Chem.* **2011**, *54*, 7464−7476.
(35) Yoshida, K.; Tanaka, S.; Yamamoto, T.; Tajima, K.; Borsali, R.; Isono, T.; Satoh, T. Chain-End Functionalization with a Saccharide

https://dx.doi.org/10.1021/acsomega.0c06316
ACS Omega 2021, 6, 7023−7033

for 10 nm Microphase Separation: ″Classical″ PS-b-PMMA versus PS-b-PMMA-Saccharide. *Macromolecules* **2018**, *51*, 8870−8877.
(36) Osaki, T.; Sunden, Y.; Sugiyama, A.; Azuma, K.; Murahata, Y.; Tsuka, T.; Ito, N.; Imagawa, T.; Okamoto, Y. Establishment of a Canine Mammary Gland Tumor Cell Line and Characterization of Its miRNA Expression. *J. Vet. Sci.* **2016**, *17*, 385−390.

https://dx.doi.org/10.1021/acsomega.0c06316
ACS Omega 2021, 6, 7023−7033